16th ICAAR LISBOA 2020-2022

16th International Conference on
Alkali-Aggregate Reaction in Concrete
Lisboa | LNEC | Portugal | 31 May - 2 June 2022

http://icaar2020-2022.lnec.pt

Detailed petrographic characterization for quantification of ASR potential of quartz-rich rocks

Aneta Kuchařová[(1)], Markéta Kuchyňová[(1)], Šárka Šachlová[(1, 2)], Richard Přikryl[(1)], Zdeněk Pertold[(1, †)]

(1) Institute of Geochemistry, Mineralogy and Mineral Resources, Faculty of Science, Charles University, Albertov 6, Prague 2, 128 43, Czech Republic, astastna@gmail.com

(2) Fuel Cycle Chemistry Department, ÚJV Řež, a. s., Hlavní 130, Řež, Husinec, 250 68, Czech Republic

Abstract

Different quartz-rich rock types from several localities in the Czech Republic and Sweden were subjected to detailed petrographic and analytical study focused on examination of their potential to alkali-silica reaction (ASR). Results were obtained by optical and electron microscopy, and petrographic image analysis, as well as by use of accelerated mortar bar test (following ASTM C1260, standard and extended time period) and accelerated concrete prism test (following RILEM AAR-4.1). The following parameters were investigated, analysed and/or quantified: microstructure, chemical and modal composition, grain size parameters and deformation features in quartz-rich rocks; and aggregate particles, cement paste, pores, alkali-silica gels, microcracks and dissolution portions in mortar and concrete samples. Except of the pegmatite quartz, all selected rocks (orthoquartzites and quartz meta-greywacke) were assigned to alkali-reactive aggregates. The highest ASR sensitivity was found to be in aggregates including cryptocrystalline matrix in significant volumes and the highest value of the ASR affected area quantified in mortar bars. The difference in expansion values of similar quartz-rich rock types (orthoquartzites) could be caused by their different microstructure (various grains size and content of cryptocrystalline matrix).

***Keywords**: aggregates; alkali-silica reactivity; expansion tests; microstructure; petrographic examination*

1. INTRODUCTION

ASR, first published by Stanton [1], was found to be one of the principal mechanisms responsible for the deterioration of various concrete structures in most countries including the Czech Republic [2, 3]. The reaction is contingent on the simultaneous presence of reactive minerals in aggregate, high alkaline conditions, and sufficient humidity [4]. Reactive forms of SiO_2 from aggregates are attacked by OH-ions finally resulting in the formation of expansive alkali-silica gels (ASGs) [5-6]. The origin of ASR causes microcracking and exfoliation of the concrete surface layers, readily visible on the micro- and macro-scale. The reactive silica may only be a minor constituent (as little as 2% in aggregate) to produce deleterious effects in concrete [7]. The highest ASR potential is connected with the amorphous and glassy character of SiO_2 (chalcedony, opal, silica glass), the poorly crystalline quartz and quartz containing lattice defects (microcrystalline, cryptocrystalline and strained quartz) as well as cristobalite and tridymite [4, 8-9]. Quartz grain size, deformation and recrystallization characteristics were suggested to be the key factors affecting the reactivity of aggregates [10-12].

Combination of the petrographic analysis (preliminary characterization of rock types by optical microscopy) with laboratory tests (mortar bars and concrete prisms tests) is the most frequently used approach in laboratory quantification of the ASR potential of aggregates [12-14]. In recent years, many researchers criticised the accelerated mortar bar test (AMBT) and concrete prism test (CPT) performed on small specimens (of basis smaller than 70 × 70 mm) due to insufficient correlation of the results with exposure of aggregate reactivity in real concrete structures [e.g., 15-16]. Moreover, severe and fast tests used solely, such as ASTM C1260-21 [17], can classify some aggregates as false non-reactive (slowly reactive aggregates) or reactive [5, 14]. The accelerated concrete test RILEM AAR-4.1 [18] has been confirmed to produce more consistent results in a relatively short time and still close to field conditions [16, 19]. This method was more effective at identifying slowly reacting aggregates [13].

The present study aimed to characterize the ASR potential of quartz-rich rocks used as aggregates by the combination of microscopic techniques and experimental tests. The RILEM AAR-4.1 [18] method was used for the first time in case of Czech aggregates.

2. EXPERIMENTAL MATERIALS

Different varieties of quartz were investigated from different rock types including: (1) well-crystallized quartz (from pegmatite, sample No. Q9) and (2) combinations of well-crystallized quartz and cryptocrystalline quartz-rich matrix (orthoquartzites - samples Nos. Q1, Q4, Q5 and quartz metagreywacke - sample No. Q7). Geological and macroscopic description was depicted in Table 2.1. All samples differ in the quartz/matrix ratio, the grain size, the presence of deformation features, as well as in the presence of accessory minerals (Table 2.2).

Table 2.1: Geological and macroscopic description of studied samples. Abbreviations: BCB - Bohemian Cretaceous Basin, BM - Bohemian Massif, BCM-Baltoscandian continental margin, CO - Caledonian Orogen, CR - Cretaceous, CZE - Czechia, JN - Jämtlandian Nappes, OR - Ordovician, PP - Paleoproterozoic, S. - sample, SO - Svecokarelian Orogen, SWE - Sweden, TBU - Teplá-Barrandian Unit. Petrographic classification was used according to Gillespie and Styles, and Robertson [20-21].

S. No.	Locality (country)	Geological unit, age	Macroscopic characterisation	Petrographic classification
Q1	SklenáHuť (CZE)	BM, TBU, OR	light grey, porous	Orthoquartzite
Q4	Jeníkov (CZE)	BM, BCB, CR	light grey, porous	Orthoguartzite
Q5	Kublov (CZE)	BM, TBU, OR	light grey, porous	Orthoquartzite
Q7	Klövsjö (SWE)	CO, BCM, JN	light white-to-yellow, massive	quartz meta-greywacke
Q9	Edsele (SWE)	SO, PP	white-to-light-yellow, massive	quartz from pegmatite

Table 2.2: Modal composition (obtained by PM-PIA, calculated according to Gillespie and Styles [20]) and petrographic characteristics (mineral phases identified by PM and SEM-EDS) of the studied aggregates. Abbreviations: AM - accessory minerals, Ap - apatite, Fm - Fe oxide-hydroxide, GB - grain boundaries, Ilt - illite, M - matrix, Mnz - monazite, Ms - muscovite, P - pore voids, Py - pyrite, Qtz - quartz, Rt - rutile, S. - sample, Ser - sericite, Ttn - titanite, Tur - tourmaline, UE - undulose extinction, Zrn - zircon.

S. No.	Modal composition (vol.%)					Qtz characteristics	M composition	AM composition
	Qtz	AM	M	P	Total			
Q1	86	1	10	3	100	Homeoblastic, fine-grained, well-visible concavo-convex (or sutured) GB	Ilt, Qtz, Rt, Ser	Ms,Mnz,Py, Rt, Ttn, Zrn
Q4	90	<1	4	5	100	Homeoblatic, very fine grained, well-visible concavo-convex GB	Fm, Qtz, Ser	Ms, Py, Rt, Tur, Zrn
Q5	89	1	6	4	100	Homeoblastic, fine grained, well-visible concavo-convex GB	Fm, Ilt, Qtz, Rt, Ser	Ap, Ms, Py, Rt, Tur, Zrn
Q7	75	<1	24	0	100	Heteroblastic, fine-grained Qtz scattered in M, partially exhibit grain-to-grain sutured GB, weak UE, diagenetic alteration	Ilt, Ms, Qtz, Ser	Ap, Rt, Zrn
Q9	99	<1	0	0	100	Undistinguishable GB (in polarizing microscope), intruded by microcracks healed by fine-grained Qtz, UE and Qtz subgrains	-	-

3. METHODS

3.1 Microscopic analyses

3.1.1 Polarizing microscopy

Polarizing microscopy (PM) was performed in the Laboratory of Microscopic Techniques (Charles University) on uncovered polished thin sections prepared from the rock samples. The cross-polarized images (XPL) were photographed with a Canon digital camera (Canon Inc., Ohta-ku, Tokyo) and then used for quantification of the rock microstructure by the petrographic image analysis (PM-PIA).

3.1.2 Electron microscopy

Scanning electron microscopy combined with energy dispersive spectrometer (SEM-EDS) was used to analyse mineral phases in the rock (e.g., accessory minerals and matrix composition), as well as in accelerated mortar bars (AMBs) and concrete prisms (CPs) (e.g., ASGs), as well as to obtained back scattered electron (BSE) images for petrographic image analysis (SEM-PIA). The polished sections (25 × 25 × 4 mm) were prepared from raw aggregates, AMBs (after 14 and 365 days of AMBT), CPs (after 20 weeks of CPT) and than coated in a carbon atmosphere. SEM-EDS was conducted at the Laboratory of Electron Microscopy and Microanalysis, Charles University (Dr. M. Racek as operator). SEM measurements were performed on a Tescan Vega instrument with an energy-dispersive analytical system (Oxford Instruments LINK ISIS 300) under the following conditions: 0.8 nA (for BSE, EDS); 120 s counting time; and accelerating voltage of 15 kV. For the standard quantitative calibration, a 53 Mineral Standard Set #02753-AB (SPI Supplies) [22] was used. For the correction of the quantitative analysis, a XPP procedure (equivalent to PAP-ϕρz) [23] was used.

3.1.3 Petrographic image analysis

PIA was performed on XPL and BSE images of polished rock sections of aggregates (PM-PIA and SEM-PIA) as well as on BSE images of AMBs (SEM-PIA) using SigmaScan® Pro v. 5.0.0 software [24]. Two types of PIA were used in this study: 1) PM-PIA using a manual outlining of objects, in which the modal composition and microstructure parameters were quantified in photographs obtained by PM of rock sections (the methodology used in this study was described elsewhere [25-26]); and 2) automated SEM-PIA was applied after the special image calibration on SEM-BSE images of rock sections, as well as AMBs (the procedure was precisely depicted in Šachlová et al. [27-28]). Different zones of backscattering contrast were distinguished in case of SEM-PIA to characterize objects in BSE images: features exhibiting a greyscale (GS) value from 0 to 70 (structural defects connected to the geological origin in rock sections and the ASR damage in AMBs), GS 71-100 (transition zone), GS 101-120 (SiO_2), GS > 120 (accessory minerals). Final ASR affected area (features connected with ASR such as dissolution gaps and microcracks) were calculated as the difference between area of GS < 70 in aggregates in AMBs and the same area in rock sections (original damage not caused by ASR as original microcracks, grain boundaries and porosity). All non-reactive minerals were excluded from SEM-PIA (areas of GS > 120). Areas including aggregate particles only were count in case of the quantification of the ASR affected area. Around ten BSE images were analysed from each section.

3.2 Experimental tests

3.2.1 ASTM C1260-21

AMBT was performed following the ASTM C1260-21 [17] standard in the Laboratory of mortar bar and concrete prism tests (Charles University). Prior to performance of the AMBT, each of the rock materials was crushed to obtain an aggregate of the desired granulometry. The mortar was then mixed using aggregate (0.125/5 mm fraction), CEM I 42.5 R cement, and distilled water in the ratio of 2.25/1/0.47 (aggregate/cement/water). Three different AMBs (in the size of 25 × 25 × 285 mm each) were prepared from each sample. After 24 hours of hardening, plus 24 hours of tempering, the AMBs were placed in 1M NaOH solution at 80°C. Expansion of AMBs was measured on three AMBs for 14 days of testing. The testing period of two AMBs was extended from the standard 14 days to one year.

3.2.2 RILEM AAR-4.1

CPT using the RILEM AAR-4.1 [18] standard was performed in the Laboratory of mortar bar and concrete prism tests (Charles University). Each of the sampled materials was crushed to obtain an aggregate of the desired granulometry. The coarse aggregate (4/22.4 mm) to fine aggregate (< 4 mm) ratio was 60:40 by mass. The real concrete mixture of aggregates (0.125/22.4 mm fraction), cement (CEM I 42.5 R, 0.77% Na_2O eq), water, plasticizer and added NaOH was calculated based on water absorption (WA), densities on an oven dry (ρ_{rd}) and saturated surface dry (ρ_{ssd}) for each sample according to the RILEM AAR-4.1 [18] standard. The alkali content of the binder was increased to 1.25% Na_2O eq (5.5 kg/m^3 Na_2O eq. of the mix) by adding calculated amount of NaOH pellets in the mix water. Determination of ρ_{rd}, ρ_{ssd} and WA of each type of the aggregate (affected the aggregate and water content added to the concrete mixture) was performed following the ČSN EN 1097-6 [29] standard. Three CPs (in the size of 75 × 75 × 290 mm) were cast from each mixture. After 24 hours of hardening

in a moist environment (> 90% RH), plus 30 min of immersing in water, the CPs were transferred to plastic sealable containers with 30 mm of water at the bottom and were placed within a reactor generating 60°C and 100% RH. No wrapping of CPs was applied in this study. CPs were removed every 5 weeks from the reactor and cooled in the sealed containers for 24 hours in a room at 20 ± 2°C. Expansion measurements were performed up to 20 weeks.

4. RESULTS

4.1 Petrographic characteristics and microstructure

Microstructure parameters were quantified separately for the rock, the quartz, and the matrix by PM-PIA (see Table 4.1). Orthoquartzites (samples Nos. Q1, Q4 and Q5) contained fine- to medium-grained quartz grains, accessory minerals, pore voids and a very fine-grained to cryptocrystalline matrix at grain interfaces (Table 4.1, Figure 4.1a-c). Quartz grains exhibited concavo-convex (or sutured) grain boundaries (Figure 4.1a-c). Composition of the matrix corresponded to a very fine-grained to cryptocrystalline quartz and minerals, which are beyond PM resolution (e.g., Fe oxide-hydroxide, illite, sericite identified by SEM-EDS) (Table 2.2). All grain size parameters (Table 4.1), as well as the amount of the matrix (Table 2.2) of orthoquartzite samples Nos. Q1 and Q5 exhibited conformable results. Sample No. Q4 exhibited slightly coarse-grained grains and lower amount of the matrix (Tables 2.2 and 4.1). The difference of orthoquartzite samples was also reflected in the specific surface. Orthoquartzite sample No. Q4 indicated the lowest value of the specific surface tot (27 for quartz) in comparison with samples Nos. Q1 and Q5 (61-62 for quartz) (Table 4.1). This was explained by its preferential concavo-convex grain boundaries and relatively high equivalent diameter. Accordingly, matrix grains indicated the highest value of the specific surface (Table 4.1). The grain size distribution expressed by the index of GSH confirmed a relatively homeoblastic fabric with equal dimensions of grains in all orthoquartzite samples (Table 4.1).

Table 4.1: Microstructure parameters measured for the whole rock (Rock), quartz (Qtz) and matrix (M) by PIA. At least 200 grains were analysed for Rock, Qtz and M in each sample. The sample Q9 was too coarse grained to microscopic measurements. Abbreviations: GSH - grain size homogeneity, Med - median, Min - minimum, Max - maximum, NA - not analysed, S. - sample, Specific Surface Tot = 4/π * ∑perimeter / ∑area. The petrographic parameters (equivalent diameter, specific surface, index of GSH) were calculated according to Dreyer and Petruk [30-31].

	Rock	Qtz	M	Rock	Qtz	M	Rock	Qtz	M	Rock	Qtz	M	Rock/ Qtz
S. No.	Q1	Q1	Q1	Q4	Q4	Q4	Q5	Q5	Q5	Q7	Q7	Q7	Q9
Area (mm^2) = the area of the analysed object													
Med	0.006	0.007	<0.001	0.032	0.033	<0.001	0.005	0.011	<0.001	0.005	0.007	<0.001	NA
Min	0.001	0.001	<0.001	0.002	0.002	<0.001	<0.001	0.0003	<0.001	<0.001	<0.001	<0.001	NA
Max	0.029	0.029	0.001	0.486	0.486	0.003	0.032	0.053	<0.001	0.169	0.169	<0.001	NA
Perimeter (mm) = the length of objects boundary													
Med	0.326	0.357	0.046	0.765	0.794	0.095	0.296	0.313	0.037	0.269	0.343	0.035	NA
Min	0.119	0.119	0.016	0.201	0.201	0.034	0.063	0.067	0.016	0.001	0.074	0.001	NA
Max	0.831	0.831	0.172	3.028	3.028	0.254	0.852	0.852	0.091	2.182	2.182	0.090	NA
Equivalent diameter (mm) = $(4 \times \text{area}/\pi)^{½}$													
Med	0.084	0.093	0.012	0.199	0.206	0.025	0.076	0.081	0.011	0.072	0.091	0.010	NA
Min	0.029	0.032	0.005	0.055	0.055	0.009	0.014	0.018	0.004	0.003	0.020	0.003	0.023
Max	0.193	0.193	0.043	0.787	0.787	0.062	0.203	0.203	0.025	0.464	0.464	0.025	>20
Specific surface (mm/mm^2) = $4/\pi \times$ perimeter/area													
Med	113	68	518	40	31	249	111	81	552	174	70	499	NA
Min	31	31	149	8	8	100	30	30	227	16	16	35	NA
Max	272	197	1239	121	121	668	598	345	1473	1207	303	1207	NA
Tot	92	61	371	34	27	206	89	62	484	145	49	448	NA
Index of GSH = average area/$\sqrt{\Sigma}$ (area of individual grain - average area)^2													
	0.072	0.074	0.065	0.055	0.055	0.115	0.055	0.058	0.100	0.016	0.049	0.070	NA

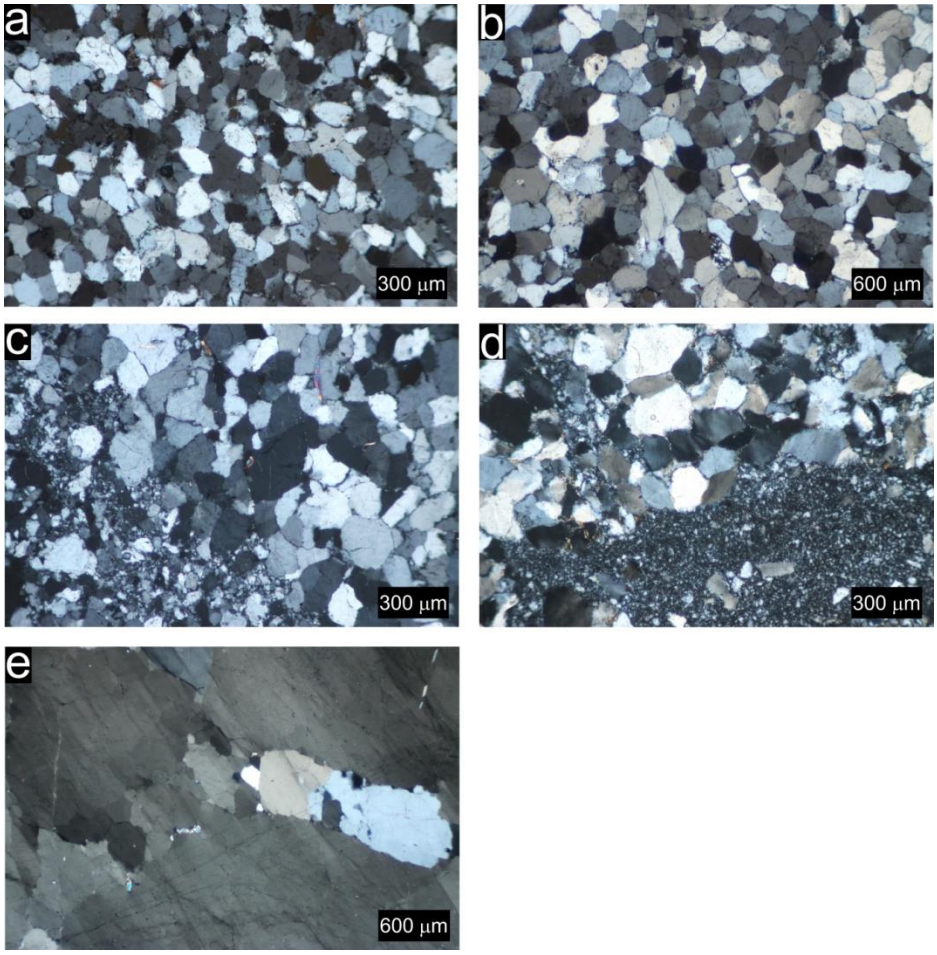

Figure 4.1: Microscopic character of investigated aggregates as seen in a polarizing microscope (crossed nicols). a orthoquartzite (sample No. Q1), b orthoquartzite (sample No. Q4), c orthoquartzite (sample No. Q5), d quartz metagreywacke (sample No. Q7), e pegmatite quartz (sample No. Q9).

Quartz meta-greywacke (sample No. Q7) included fine-grained quartz grains scattered in the very fine-grained to cryptocrystalline matrix and accessory minerals (Table 2.2, 4.1). Quartz grains exhibited partially grain-to-grain sutured boundaries, weak undulose extinction and diagenetic alteration (Figure 4.1d). The matrix was composed of a very fine-grained to cryptocrystalline quartz and other minerals such as illite and muscovite identified by SEM-EDS (Table 2.2). The specific surface of the quartz meta-greywacke was higher than this parameter of orthoquartzite samples (145 for the whole rock) (Table 4.1). The main influence could be found in sutured grain boundaries and higher amount of the matrix of the quartz meta-greywacke in comparison with orthoquartzite samples. However, the specific surface tot value of matrix grains was conformable in all the studied samples except the slightly coarse grained orthoquartzite sample No. Q4 (Table 4.1). The grain size distribution of the quartz meta-greywacke (sample No. Q7) expressed by the lowest value of the index of GSH (0.02 for the rock) reflected a heteroblastic fabric with different dimensions of grains. However, the matrix grains indicated homeoblastic fabric as for all the studied samples (see Table 4.1). Quartz from pegmatite (sample No. Q9) was very coarse-grained with grain boundaries not possible to be observed using the naked-eye or captured in PM (microstructure parameters were not quantified by PM-PIA). Large quartz grains (equivalent diameter greater than 2 cm) were penetrated by microcracks healed by fine-grained quartz (Fig. 4.1e). The undulose extinction and the origin of quartz subgrains were observed in most of the coarse quartz grains.

4.2 ASR potential according to expansion tests

Šachlová et al. [27] reported expansion data of AMBT following the ASTM C1260-21 [17] standard after 14 days except of the orthoquartzite sample No. Q4. Referred to the test, almost all studied samples (Nos. Q1, Q4, Q5, Q7) can be classed as alkali-reactive aggregates (expansion of AMBs greater than

0.10% after 14 days and greater than 0.20% after 28 days), except the pegmatite quartz (sample No. Q9) exhibiting the lowest expansion value (0.08% after 14 days) (Table 4.2, Figure 4.2a). The highest expansion value was measured for the quartz metagreywacke (sample No. Q7) which finally reached 2.22% when the standard AMBT was prolonged to one year (Table 4.2).

Table 4.2: Mean expansion values of AMBs according to ASTM C1260-21 [17] after 14 (AMBT 14), 28 (AMBT 28), 365 (AMBT 365) days, and CPs according to RILEM AAR-4.1 [18] after 15 (CPT 105) and 20 (CPT 140) weeks. Abbreviation: S. - sample.

S. No.	Mean expansion (%)				
	AMBT 14	AMBT 28	AMBT 365	CPT 105	CPT 140
Q1	0.245	0.451	1.768	0.038	0.042
Q4	0.190	0.271	1.261	0.014	0.018
Q5	0.221	0.346	1.327	0.011	0.012
Q7	0.418	0.549	2.222	0.051	0.051
Q9	0.080	0.162	1.234	0.049	0.074

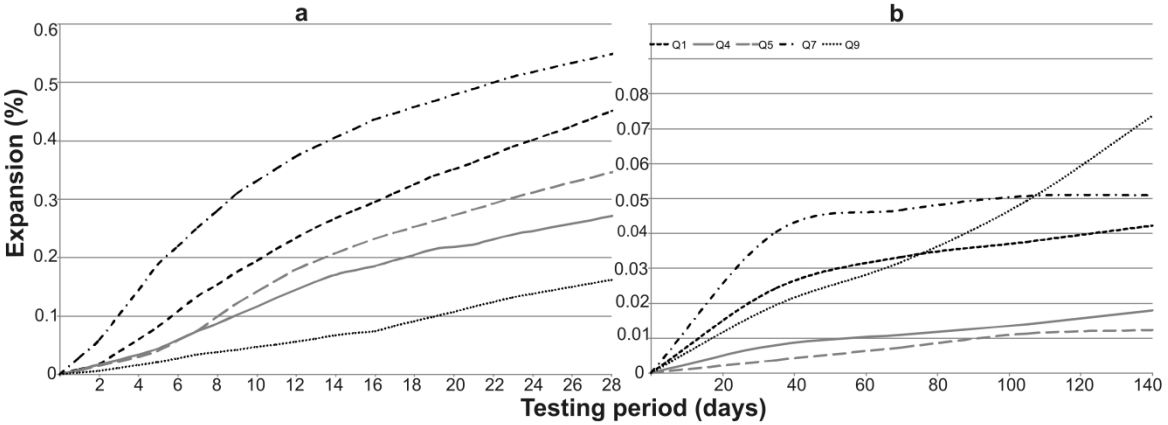

Figure 4.2: Expansion curves of a) AMBs (according to ASTM C1260-21 [17]) and b) CPs (according to RILEM AAR-4.1 [18]). Samples Nos. Q1, Q4 and Q5 (orthoquartzites), Q7(quartz metagreywacke), Q9 (pegmatite quartz). The limit of 0.1 % (in case a, after 14 days) and 0.03 % (in case b, after 140 days) is the value dividing non-reactive and reactive aggregates.

CPT following the RILEM AAR-4.1 [18] standard was used as added method to the AMBT. Based on the test, expansions of less than 0.03 % after 20 weeks indicated that the aggregate can be regarded as non-reactive [13]. Samples Nos. Q1, Q7 and Q9 exceeded the limit in case of results of our study (Table 4.2, Figure 4.2b). Lower expansion values were measured for orthoquartzite samples Nos. Q4 and Q5 (Table 4.2).

4.3 Description and quantification of ASR products in mortar bars and concrete prisms

Orthoquartzites (samples Nos. Q1, Q4 and Q5) exhibited specific dissolution of fine grained to cryptocrystalline matrix around quartz grains. The dissolution “net” was extensively developed in the cement rims around quartz grains of aggregate particles of AMBs (Figure 4.3b, f, j), as well as on aggregate tested by CPT (Figure 4.3d, h, l). Total amount of ASR affected area was calculated among 1 and 5 vol.% after 14 days of AMBT (Table 4.3). Individual ASGs took from 0.2 to 1.3 vol.% in the cement paste and pores. Large dissolution gaps, extension of microcracks and ASGs in aggregate particles, as well as the silicification of the cement paste were observed in AMBs stored one year in the alkaline solution (Figure 4.3c, g, k). ASGs were predominantly located in cement / aggregate boundaries in case of CPs (Figure 4.3h). The quartz metagreywacke (sample No. Q7) was characterized by larger ASR damage observed in AMBs (7 vol.% of ASR affected area) (Table 4.3) and CPs in comparison with other studied samples. Partially or complete dissolution of cryptocrystalline matrix, included herein significant volume (24 vol.%) (Table 2.2), and frequent ASGs in pores and microholes (1.4 vol.%) were observed in AMBs (Figure 4.3n, Table 4.3). Moreover, complete dissolution of some aggregate particles was exhibited from long-term storage in the alkaline solution (Figure 4.3o).

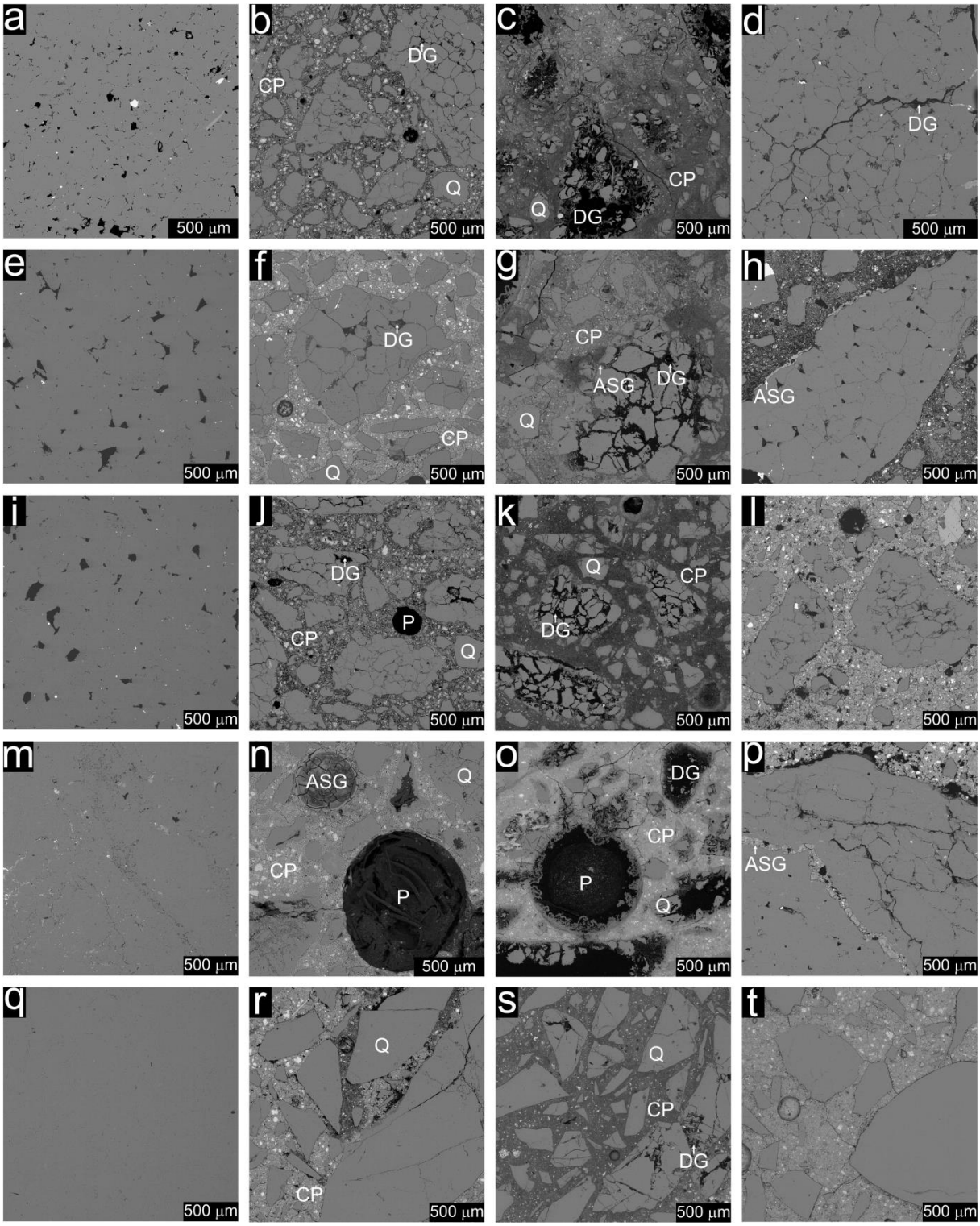

Figure 4.3: SEM-BSE microphotographs from rock sections (a, e, i, m, q); AMBs (after 14 days - b, f, j, n, r; and after one year - c, g, k, o, s); and CPs (d, h, l, p, t). a-d orthoquartzite (sample No. Q1), e-h orthoquartzite (sample No. Q4), i-l orthoquartzite (sample No. Q5), m-p quartz metagreywacke (sample No. Q7), q-t pegmatite quartz (sample No. Q9). Abbreviations: ASG - alkali-silica gel, CP - cement paste, DG -dissolution gap, Q - quartz, P - pore.

BSE images of CPs showed similar ASR signs in aggregates as in AMBs but to a lesser extent. However, ASGs were frequently located in cement/aggregate boundaries or in microcracks of aggregates (Figure 4.3p) in CPs. Pegmatite quartz (sample No. Q9) exhibited lower amount of ASR

affected area (2 vol. % after 14 days of AMBT) in comparison with other studied samples (Table 4.3). Individual ASGs filled only 0.4 vol.% in the cement paste and pores (Table 4.3). The extension of original microcracks and formation of new microcracks located probably in quartz subgrains were observed in AMBs and less common in CPs (Figure 4.3r, t). One year immersion in the alkaline solution brought about larger dissolution gaps in aggregates and silicification of the cement paste of AMBs (Figure 4.3s).

Table 4.3: Areas in polished rock samples (rock) and in AMBs after 14 days (AMBT 14) quantified by SEM-PIA in vol.%. ASR affected area in aggregates was calculated as area of GS value < 70 in AMBs minus the same area counted in rock samples. Abbreviations: CP - cement paste, S. - sample.

S. No.	Aggregate area	CP area	Empty pores	ASG in pores	ASG in CP	Total area	GS 0-70 area in aggregates	ASR affected area in aggregates
Q1 AMBT 14	52.03	43.15	4.07	0.69	0.06	100.00	6.21	0.72
Q1rock							5.48	
Q4 AMBT 14	54.91	42.80	2.10	0.16	0.03	100.00	5.81	1.94
Q4rock							3.87	
Q5 AMBT 14	58.78	37.26	2.63	1.29	0.05	100.00	8.11	5.01
Q5 rock							3.10	
Q7 AMBT 14	56.01	40.22	2.33	1.40	0.04	100.00	9.30	7.43
Q7 rock							1.87	
Q9 AMBT 14	54.96	42.51	2.18	0.33	0.02	100.00	2.99	2.04
Q9 rock							0.95	

4.4 Chemical composition of alkali-silica gels

Variability in the chemical composition of ASGs detected in AMBs and CPs was depicted in Table 4.4. ASGs of AMBs (after 14 and 365 days of testing) showed wider range of prevailing SiO_2 (39-70 wt.%) than ASGs of CPs (46-60 wt.%). Chemical composition of ASGs of AMBs corresponded to Si-Ca-Na gel with very low content of MgO, K_2O, SO_3, Al_2O_3 and FeO. The one-year storage in the alkaline solution induced significant Na enrichment (Ca depletion) of ASGs (Na_2O of 13-20 wt.%) in comparison with ASGs in AMBs after 14 days (Na_2O of 3-10 wt.%) (Table 4.4). On the other hand, chemical composition of ASGs of CPs corresponded to Si-Ca-K gel with very low content of Na_2O, SO_3, MgO, FeO and Al_2O_3.

Table 4.4: Semi-quantitative SEM-EDS measurements of selected ASGs (in wt.%) analysed in AMBs according to ASTM C1260-21 [17] after 14 (AMBT 14), 365 (AMBT 365) days, and CPs according to RILEM AAR-4.1 [18] after 20 (CPT 140) weeks. Abbreviations: TM - testing method, S. - sample.

S. No	TM	Na_2O	MgO	Al_2O_3	SiO_2	SO_3	K_2O	FeO	CaO	Total
Q1	AMBT 14	4.66	0.49	0.18	54.11	0.00	1.17	0.00	16.90	77.51
Q1	AMBT 14	4.96	1.58	0.10	54.83	0.00	1.03	0.00	14.78	77.28
Q1	AMBT 365	13.41	0.47	0.06	52.76	0.00	0.00	0.00	13.66	80.36
Q1	AMBT 365	19.65	0.59	1.30	53.89	0.00	0.52	0.00	8.40	84.34
Q1	CPT 140	2.30	0.08	1.78	58.15	0.00	6.28	0.16	19.41	88.16
Q1	CPT 140	1.13	0.00	0.00	59.42	0.00	3.14	0.00	24.26	87.95
Q4	AMBT 14	6.87	0.85	0.49	41.53	0.38	0.51	0.00	25.40	76.02
Q4	AMBT 14	4.10	1.30	1.32	38.86	0.29	0.41	0.00	21.48	67.77
Q4	AMBT 365	16.54	0.40	0.12	45.85	0.00	0.00	0.00	11.48	74.39
Q4	AMBT 365	15.71	0.34	0.04	46.11	0.00	0.00	0.00	12.37	74.57
Q4	CPT 140	1.24	1.05	0.11	45.68	0.00	4.78	0.00	27.62	80.48
Q4	CPT 140	1.16	0.41	0.08	52.00	0.00	6.00	0.00	25.11	84.76
Q5	AMBT 14	4.91	0.76	0.43	54.24	0.00	0.77	0.00	19.62	80.73
Q5	AMBT 14	3.10	0.70	0.26	60.34	0.00	0.84	0.00	13.82	79.06
Q5	AMBT 365	13.11	0.28	0.23	60.20	0.00	0.14	0.00	15.59	89.54
Q5	AMBT 365	13.31	0.40	0.13	52.69	0.00	0.00	0.00	12.19	78.71
Q5	CPT 140	1.36	0.00	0.00	54.84	0.00	6.62	0.00	16.12	78.94
Q5	CPT 140	1.13	0.00	0.07	56.33	0.00	4.07	0.00	23.59	85.20
Q7	AMBT 14	5.82	0.80	0.16	70.29	0.00	1.57	0.16	9.63	88.44
Q7	AMBT 14	7.54	0.16	0.02	62.43	0.00	1.50	0.00	17.81	89.46
Q7	CPT 140	0.45	0.10	0.11	57.38	0.00	1.60	0.00	26.36	86.00
Q7	CPT 140	1.54	0.14	0.03	57.43	0.00	4.09	0.00	22.25	85.49
Q9	AMBT 14	10.06	0.89	0.43	63.47	0.00	0.23	0.00	11.89	86.97
Q9	AMBT 14	4.57	0.63	0.98	60.85	0.00	0.35	0.00	8.84	76.22
Q9	CPT 140	1.11	0.68	1.18	51.75	0.84	1.90	0.18	22.99	80.65
Q9	CPT 140	3.39	0.51	1.61	60.28	0.00	8.09	1.18	18.65	93.71

5. DISCUSSION

Expansion values of AMBs were compared with the percentage of ASR affected area in aggregates in AMBs, as well as with the amount of cryptocrystalline matrix in rock sections. The linear correlation was found in both cases (Figure 5.1). However, the orthoquartzite sample No. Q1 was not included in the comparison between the expansion and the ASR affected area because of its poor correlation (Figure 5.1a). The possible explanation probably consists in a selection of the rock section affected extensively by original geological microcracks and porosity which overestimated the value of the GS-70 area in aggregates (caused the lowest value of ASR affected area - 0.72 vol.%) calculated by SEM-PIA (Table 4.3). This fact was confirmed by Šachlová et al. [28] who obtained the higher and correlative value of the ASR affected area (5.8 vol.%) of another sample from the same locality. The area of cryptocrystalline matrix of rocks approximately corresponded with areas of main dissolution gaps in aggregates of AMBs (Figure 4.1 vs. Figure 4.3). The alkaline etching of cement rims located along grain boundaries of orthoquartzites were already demonstrated on rock samples underwent the etching experiment by Šachlová et al. [27]. Expansion values of AMBs of all orthoquarzite samples were in agreement with the grain size (sample No. Q4 displayed the highest grain size and the lowest expansion among orthoquarzites) and the amount of cryprocrystalline matrix (sample No. Q1 exhibited the highest amount of cryptocrystalline matrix and expansion of AMBs among orthoquarzites) (Tables 2.2, 4.1, 4.2). The similar positive correlation between the content of reactive quartz and the expansion of AMBs was found in the study of siliceous sands used as fine aggregates by Antolik et al. [32]. The petrographic characteristics correlated better with results of the AMBT than with the CPT in this study. This is in contradiction with results for slowly reactive aggregates as was described by Ramos et al. [14]. The expansion curves of CPs of orthoquarzites (samples Nos. Q1, Q4, Q5) and the quartz metagreywacke (sample No. Q7) displayed similar trends as AMBs (Figure 4.2). However, two orthoquarzites (samples Nos. Q4, Q5) were classed as non-reactive according to the RILEM AAR-4.1 method [13]. Generally, an underestimation of the true expansion level could result from the leaching of alkalis included in CPs. This problem, connected mainly with laboratory tests, has been widely discussed [33-34]. However, the stronger alkali leaching of the two samples is improbable compared to the rest of samples in this case (known mineralogical composition of aggregates, identical pre-storage and storage conditions). The steep expansion curve of the pegmatite quartz (sample No. Q9) with the highest expansion value (0.074% after 20 weeks) of CPs could be explained by higher sensitivity of the CPT to detect microcracks content including fine-grained quartz in this sample.

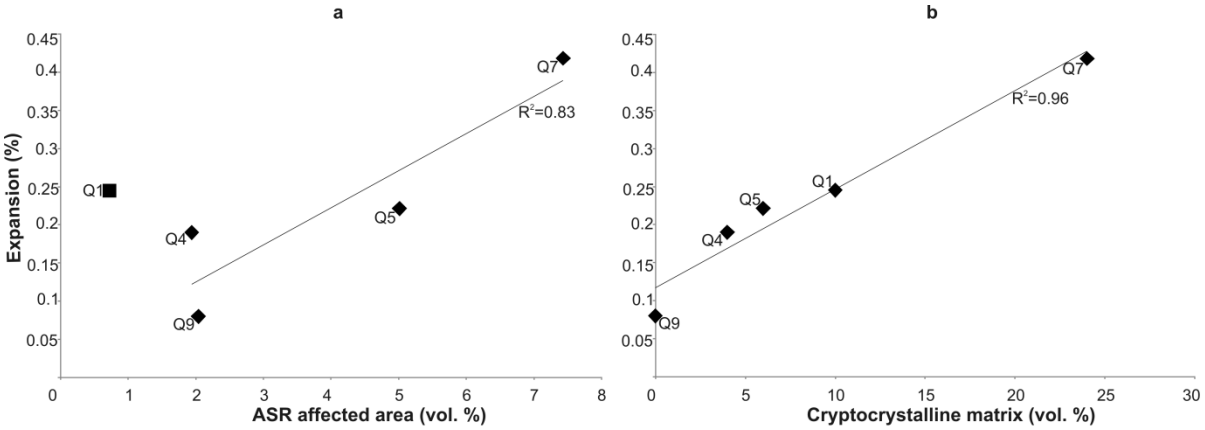

Figure 5.1: Correlation of ASR affected area values (a) and cryptocrystalline matrix content (b) with expansion values of AMBs (ASTM C1260-21, 14 days). Sample Nos. Q1, Q4 and Q5 (orthoquartzites), Q7(quartz metagreywacke), Q9 (pegmatite quartz). The R^2 value of the correlation was calculated only for samples Nos. Q4 - Q7 in case of the portion a.

Similar values were obtained for slowly reactive granitic rocks by Ramos et al. [14]. An application of the RILEM AAR-4.1 [18] method to more samples would be necessary to elucidate this behaviour.

SEM-EDS analyses divided ASGs into Na, Ca-rich ASGs (in case of AMBs) and K, Ca-rich ASGs (in case of CPs) (Figure 5.2a). The composition of ASGs thus well reflected surrounding conditions of their origin either in AMBs (accelerating solution composed of NaOH as unlimited source of Na) or in CPs

(cement paste, added NaOH and plasticizer as possible sources of Na^+, Ca^{2+}, K^+). Moreover, SEM-EDS measurements of ASGs (Table 4.4) are in agreement with their location in mortar or concrete. The Ca content is generally more prevalent in microcracks of ASGs found in the cement paste than inside aggregates [35]. Based on our study, ASGs were found predominantly in microcracks between the cement paste and aggregates (in CPs) or in pores of cement paste (in AMBs) (Figure 4.3h, n). Na-enriched as well as Ca-depleted ASGs were identified in AMBs after one year of testing caused by its long time immersion in NaOH solution (Figure 5.2).

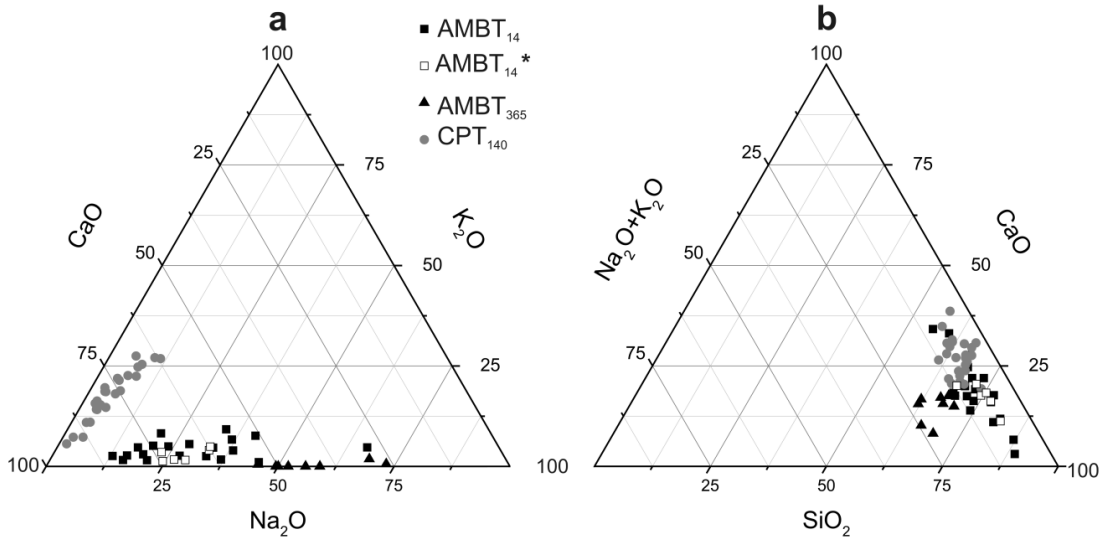

Figure 5.2: Ternary diagrams of Na_2O-K_2O-CaO (a) and SiO_2-CaO-(Na_2O+K_2O) (b) of all ASGs analysed in AMBs (ASTM C1260-21: 14 days - $AMBT_{14}$ and one year - $AMBT_{365}$) and CPs (RILEM AAR-4.1: 20 weeks - CPT_{140}); *data of these ASGs were adopted from Šachlová et al. [28].

6. CONCLUSIONS

Based on the combination of detailed petrographic examination and expansion tests, almost all studied samples (orthoquartzites and quartz meta-greywacke) can be assigned to alkali-reactive aggregates, except the pegmatite quartz. The highest ASR potential was assigned to quartz meta-greywacke. This was explained by presence of the highest amount of cryptocrystalline matrix (quantified in rocks) and the ASR affected area (quantified in AMBs). The petrographic characteristics were in agreement with the AMBT (ASTM C1260-21) and CPT (RILEM AAR-4.1) in which the quartz meta-greywacke exceeded their limits. The orthoquartzites varied in the degree of reactivity according to their different microstructure (grain size and amount of cryptocrystalline matrix). All types of orthoquartzites were determined as alkali-reactive based on the AMBT and CPT, except the two types (samples Nos. Q4, Q5) classed as non-reactive according to the RILEM AAR-4.1 test. The conflicting results of orthoquartzites in these standard testing methods was not explained (the implication of alkali leaching was discussed). Another problem was low quantification of the ASR affected area in the sample No. Q1 in AMBs connected with a possible overestimation of original defects in the rock by SEM-PIA. The example confirmed the requirement of accurate input data for the PIA. Pegmatite quartz indicated the low ASR potential on account of petrographic characteristics and the AMBT. However, the expansion value of the CPT (the highest from all samples) pointed to slowly reactive aggregate. The long-term storage of all AMBs in the alkaline solution was reflected mainly in: (1) the extension of dissolution gaps, microcracks and ASGs, (2) the silicification of the cement paste and (3) the Na enrichment (Ca depletion) of ASGs.

7. ACKNOWLEDGEMENTS

The study was financially supported from the research project No. GA21-26542S. Special thanks belong to Prof. Karel Miskovsky from Envix Nord AB (Sweden) for his assistance with the selection of Swedish samples. In Memoriam of Prof. Zdeněk Pertold (1933-2020), an outstanding scholar and dear friend.

8. REFERENCES

[1] Stanton TE (1940) Expansion of concrete through reaction between cement and aggregate. Proceedings of the American Society of Civil Engineers 66(10):1781-1811.

[2] Lukschová Š, Přikryl R, Pertold Z (2009) Petrographic identification of alkali-silica reactive aggregates in concrete from 20th century bridges. Constr Build Mat 23(2):734-741. https://doi.org/10.1016/j.conbuildmat.2008.02.020

[3] Sims I, Poole A (2017) Alkali-Aggregate Reaction in Concrete: A World Review. Taylor and Francis Group, London

[4] Fernandes I, Broekmans MATM (2013) Alkali-Silica Reactions: An Overview. Part I. Metallography, Microstructure and Analysis 2:257-267. https://doi.org/10.1007/s13632-013-0085-5

[5] Figueira RB, Sousa R, Coelho L, Azenha M, de Almeida JM, Jorge PAS, Silva CJR (2019) Alkali-silica reaction in concrete: Mechanisms, mitigation and test methods. Construction and Building Materials 222:903-931. https://doi.org/10.1016/j.conbuildmat.2019.07.230

[6] Rajabipour F, Giannini E, Dunant C, Ideker JH, Thomas MDA (2015) Alkali–silica reaction: Current understanding of the reaction mechanisms and the knowledge gaps. Cement and Concrete Research 76:130-146. https://doi.org/10.1016/j.cemconres.2015.05.024

[7] Poole AB (2017) Introduction, Chemistry and Mechanisms. In: Sims I, Poole A (eds) Alkali-Aggregate Reaction in Concrete: A World Review. Taylor and Francis Group, London, pp 1-31

[8] Broekmans MATM (2004) Structural properties of quartz and their potential role for ASR. Materials Characterization 53(2-4):129-140. https://doi.org/10.1016/j.matchar.2004.08.010

[9] Locati F, Marfil S, Baldo E (2010) Effect of ductile deformation of quartz-bearing rocks on the alkali-silica reaction. Engineering Geology 116(1-2):117-128. https://doi.org/10.1016/j.enggeo.2010.08.001

[10] Wenk HR, Monteiro PJM, Shomglin K (2008) Relationship between aggregate microstructure and mortar expansion. A case study of deformed granitic rocks from the Santa Rosa mylonite zone. Journal of Materials Science 43(4):1278-1285. https://doi.org/10.1007/s10853-007-2175-8

[11] Wigum BJ (1995) Examination of microstructural features of Norwegian cataclastic rocks and their use for predicting alkali-reactivity in concrete. Engineering Geology 40(3-4):195-214. https://doi.org/10.1016/0013-7952(95)00044-5

[12] Castro N, Wigum BJ (2012) Assessment of the potential alkali-reactivity of aggregates for concrete by image analysis petrography. Cementand Concrete Research 42(12):1635-1644.https://doi.org/10.1016/j.cemconres.2012.08.009

[13] Lindgård J, Nixon PJ, Borchers I, Schouenborg B, Wigum BJ, Haugen M, Åkesson U (2010) The EU “PARTNER” Project -European standard tests to prevent alkali reactions in aggregates: final results and recommendations. Cement and Concrete Research 40 (4): 611-635. https://doi.org/10.1016/j.cemconres.2009.09.004

[14] Ramos V, Fernandes I, Silva AS, Soares D, Fournier B, Leal S, Noronha F (2016) Assessment of the potential reactivity of granitic rocks - Petrography and expansion tests. Cement and Concrete Research 86:63-77. https://doi.org/10.1016/j.cemconres.2016.05.001

[15] Fernandes I, Broekmans MATM, Nixon P, Sims I, Ribeiro MA, Noronha F, Wigum B (2013) Alkali-silica reactivity of some common rock types - a global petrographic atlas. Quarterly Journal of Engineering Geology and Hydrogeology 46:215-220. https://doi.org/10.1144/qjegh2012-065

[16] Lindgård J, Thomas MDA, Sellevold EJ, Pedersen B, Andiç-Çakır Ö, Justnes H, Rønning TF (2013) Alkali-silica reaction (ASR)-performance testing: Influence of specimen pre-treatment, exposure conditions and prism size on alkali leaching and prism expansion. Cement and Concrete Research 53:68-90. https://doi.org/10.1016/j.cemconres.2013.05.017

[17] ASTM C1260-21 (2021) Standard Test Method for the Potential Alkali Reactivity of Aggregates (Mortar-Bar Method). The American Society for Testing and Materials, Philadelphia, USA, pp 1-5

[18] RILEM AAR-4.1 (2016) RILEM Recommended Test Method: AAR-4.1-Detection of Potential Alkali-Reactivity-60 °C Test Method for Aggregate Combinations Using Concrete Prisms. In: Nixon PJ, Sims I (eds) RILEM Recommendations for the Prevention of Damage by Alkali-Aggregate Reactions in New Concrete Structures. RILEM State-of-the-Art Reports, 17. Springer, Dordrecht, pp 99-116

[19] Yamada K, Karasuda S, Ogawa S, Sagawa Y, Osako M, Hamada H, Isneini M (2014) CPT as an evaluation method of concrete mixture for ASR expansion. Construction and Building Materials 64:184-191.https://doi.org/10.1016/j.conbuildmat.2014.04.034

[20] Gillespie MR, Styles MT (1999) BGS Rock Classification Scheme. Volume 1. Classification of Igneous Rocks. British Geological Survey, Nottingham, UK. Report No.: RR 99-06

[21] Robertson S (1999) BGS rock classification scheme. Volume 2. Classification of metamorphic rocks. British Geological Survey, Nottingham, UK. Report No.: RR 99-02

[22] SPI Supplies (2021) http://www.2spi.com. Accessed 27 December 2021

[23] Pouchou J, Pichoir F (1985) PAP" (ϕρz) procedure for improved quantitative microanalysis. In: Armstrong JT (ed) Microbeam Analysis. San Francisco Press, San Francisco, pp 104–106

[24] SPSS Software (2021) SigmaScan®ProV 5.0. https://systatsoftware.com/sigmascan-pro/. Accessed 27 December 2021

[25] Přikryl R (2001) Some microstructural aspects of strength variation in rocks. Int J Rock Mech Mining Sci GeomechAbstr 38(5):671-682. https://doi.org/10.1016/S1365-1609(01)00031-4

[26] Přikryl R (2006) Assessment of rock geomechanical quality by quantitative rock fabric coefficients: Limitation and possible source of misinterpretations. Engineering Geology 87(3-4):149-162.https://doi.org/10.1016/j.enggeo.2006.05.011

[27] Šachlová Š, Kuchařová A, Pertold Z, Přikryl R (2016) Evaluation of alkali-silica reaction potential of quartz-rich rocks by alkaline etching of polished rock sections. Environmental Earth Sciences 75(9):1-14. https://doi.org/10.1007/s12665-016-5519-3

[28] Šachlová Š, Kuchařová A, Pertold Z, Přikryl R, Fridrichová M (2017) Quantitative assessment of alkali silica reaction potential of quartz-rich aggregates: comparison of chemical test and accelerated mortar bar test improved by SEM-PIA. Bull Eng Geol Env 76(1):133-144.https://doi.org/10.1007/s10064-015-0812-z

[29] ČSN EN 1097-6 (2001) Testing of mechanical a physical properties of aggregates (In Czech). Czech office for standards, metrology and testing, pp 1-40

[30] Dreyer W (1973) The science of rock mechanics. Part I. The strengthproperties of rocks. Series on rock and soil mechanics, 2nd edn.Trans Tech, Clausthal

[31] Petruk W (1986) Image analysis: an overview of developments. CANMET Report 86-4E

[32] Antolik A, Jóźwiak-Niedźwiedzka D, Dziedzic K,Bogusz K, Glinicki MA (2020) Microscopic analysis of the alkali-silica reactivity of various origin fine aggregate. MATEC Web of Conferences 322:1-8. https://doi.org/10.1051/matecconf/202032201025

[33] Lindgård J, Andiç-Çakır Ö, Fernandes I, Rønning TF, Thomas MDA (2012) Alkali–silica reactions (ASR): Literature review on parameters influencing laboratory performance testing. Cement and Concrete Research 42(2):223-243. https://doi.org/10.1016/j.cemconres.2011.10.004

[34] Costa U, Mangialardi T, Paolini AE (2017) Minimizing alkali leaching in the concrete prism expansion test at 38 degrees C. Construction and Building Materials 146:547-554. https://doi.org/10.1016/j.conbuildmat.2017.04.116

[35] Knudsen T, Thaulow N (1975) Quantitative micro analyses of alkali-silica gel in concrete. Cement and Concrete Research 5:443-454. https://doi.org/10.1016/0008-8846(75)90019-8